Strengthening mechanism and properties of Co–WC composite coatings deposited by plasma-transferred arc welding

Qiuyue Jiang[1], Ye Tian[2], Fengyuan Shu[2] ✉, Hongyun Zhao[2], Yiming Sun[2], Wenxiong He[2], Binshi Xu[3]

[1]*Institute of Technology, School of Mechanical and Electrical Engineering, Changchun University of Technology, Changchun 130012, People's Republic of China*
[2]*Shandong Provincial Key Laboratory of Special Welding Technology, Harbin Institute of Technology at Weihai, Weihai 264209, People's Republic of China*
[3]*National Key Laboratory for Remanufacturing, Beijing, 100072, People's Republic of China*
✉ *E-mail: shufengyuan@163.com*

Published in Micro & Nano Letters; Received on 10th September 2018; Revised on 18th February 2019; Accepted on 25th February 2019

Cobalt (Co)-based tungsten carbide (WC) wear-resistant coatings with different content of WC were prepared on the surface of Q235 low carbon steel by plasma-transferred arc welding. The properties of the coatings such as strengthening mechanism, microhardness and wear properties were tested by using a metallurgical microscope, scanning electron microscope, energy dispersive spectrometer, X-ray diffraction, Rockwell hardness tester, and friction wear equipment. The results show that the main reasons for the strengthening of spray welding layer are the solution strengthening formed by α-Co with supersaturated tungsten (W) and the dispersion strengthening caused by eutectic precipitated carbide and silicide. The proportion of the solid solution of W in α-Co steadily ranges from 18.00 to 19.59%. The morphologies of rich W-phase are mainly related to the content of W. With the content of W increasing, the evolution process of the shape is the amorphous form→damascene shape→star-like shape→the polygon. Amorphous W-rich phase can be obtained when the content of WC ranges from 20 to 30%, evenly distributed W-rich phase in the shape of damascene or star can be obtained when the WC content ranges from 30 to 40%, and the polygonal W-rich phase can be obtained at the percentage of 40–50%.

1. Introduction: With the development of oil and mineral exploitation industry, machinery industry has a higher requirement on the material performance index. During the production, long-term workload contributes to the surface failure of many key parts. Thus, it appears a high application value to improve the surface performance of key components [1]. Surface strengthening technology, which enhances the abrasive resistance of the surface, arises at the historic moment to solve the dilemma. Techniques such as thermal spraying [2, 3], laser cladding [4–6], electron beam-physical vapor deposition (EB-PVD) [7] and surface overlaying [8] can improve the surface performance of components such as abrasive resistance and corrosion resistance. Spray welding is one of the widely used surface techniques [9, 10], and surface spray welding wear-resistant alloy layer is the major research direction at the present stage.

Spray welding layer of cobalt-base alloy has characteristics of excellent high temperature impact wear resistance and outstanding high temperature oxidative stability [11]. This study is mainly focused on cobalt–tungsten carbide (Co–WC) powder, utilising the spray welding technique with optimised parameters to prepare Co–WC composite wears resistant coatings on Q235 steel, and studies the influence of WC powder content variation on the morphology of spray welding layer. It is proved that the strengthening of the plasma spray welding layer is a joint effort of solid solution strengthening and second phase precipitation strengthening. With the WC content increasing in spray welding layer, the dissolving and precipitating behaviour of WC and the variation of carbide's types and forms generated during the process is analysed in this study. Combined with the strengthening effects of other elements on the spray welding layer, the change regulation of the strengthening mechanism of the spray welding layer is demonstrated.

2. Experimental methods and materials

2.1. Substrate and spray welding powder: The substrate was Q235-B steel. The composition of as-received Q235 steel is 0.14–0.22 C, 0.30–0.65 Mn, ≤0.30 Si, ≤0.045 P, ≤0.055 S, Fe rest (wt.%). The powder for spray welding was FCo-06 high temperature self-fluxed alloy powder, which was in the shape of an ellipsoid, with the melting point of 1035–1150°C and the particle size range of −60 to +150 mesh. The powder had superior performance in heat-resisting, wear-resisting, anti-corrosion, anti-oxidation etc. The main composition of the powder was Co, Cr and W. The WC powder used was FZWC (cast WC powder), which was mostly in the shape multi-prismatic with the melting point of 2525°C and the particle size range of −200 to +400 mesh. The cast WC could be applied to the strengthening of the petroleum drilling tool, building material machinery and other devices easy to fray. The chemical compositions of FCo-06 and FZWC are shown in Tables 1 and 2, respectively.

2.2. Experimental equipment and process: The spray welding experiment was completed by numerical controlled multi-function powder plasma spray welding machine made by Beijing Chenkaile Technology Co. Ltd. The powder feeding system of the spray welding machine used scraper powder feeding device with gas assisted to send powder. The flow of powder feeding could be changed by controlling the leak hole diameter and revolving speed of the rotating platform. As shown in Table 3, there were seven types of Co-based alloy powder with different proportion used in the spray welding experiments.

The Q235 steel was processed to samples with dimensions of 100 mm × 100 mm × 6 mm by plate shearing machine. The surfaces of samples were sanded by an abrasive paper to remove rust and washed by acetone. Before the spray welding experiment, the substrate was preheated to 90–150°C. The optimised parameters of the spray welding were spray welding current of 60–65A, spray welding voltage of 48 V, plasma gas flow (Ar) of 3.5 l/min, powder feeding flow of 5–6 l/min, spray welding speed of 100 mm/min. Also, the height from the nozzle to the surface of the substrate was 10 mm. Seven types of powder were all uniformly mixed by the way of ball-milling. The optimised parameters of the

Table 1 Chemical compositions of FCo-06 (wt%)

Si	B	Cr	Ni	W	Co
3.5–4.5	2.5–3.5	28–32	10–12	5–6	bal

Table 2 Chemical compositions of FZWC (wt%)

Total C	Free C	O	W
3.7–4.0	≤0.08	≤0.20	bal

Table 3 Different compositions of powder (wt%)

Number	A_1	A_2	A_3	A_4	A_5	A_6
WC content	10	20	30	40	50	60

ball-milling were grinding ball diameter of 10 mm, ball-to-powder weight ratio of 8:1, milling velocity of 100 rpm, milling time of 2 h.

2.3. Experimental analysis: Metallographic specimens with dimensions of 5 mm × 10 mm × 12 mm were cut out along the vertical direction of spray welding by cutting machine, and then were sanded by an abrasive paper from 180# to 1200# successively and polished by polishing machine. After the samples were corroded by dilute aqua regia (50% nitric acid + 25% hydrochloric acid + 25% water) for 8–10 s, the morphology of the spray welding layer was observed under the Olympus optical microscope. The phase was analysed by X-ray diffraction (XD-2 type), the back-scattering images were obtained by using a scanning electron microscope (VEGA II SBH type), and the composition of the generated phase was analysed by energy dispersive spectroscopy (EDS).

3. Analysis for strengthening mechanism of the spray welding layer

3.1. Solid solution strengthening of Co-based solid solution: The solid solution strengthening of Co-based alloy is mainly reflected by the strengthening effect of the α-Co-based solid solution. Fig. 1 shows the X-ray diffraction (XRD) test results of A_1–A_6.

It can be obtained from the XRD results of A_1–A_6 that α-Co mainly forms solid solution (α-Co, γ-Fe) with Fe element because of the dilution effect of the substrate. Instead of CoCr phase, Co_3Fe_7 phase and CoFe phase are main existing forms. Since the α-Co-based solid solution has a face-centred cubic austenite structure, whose diffusion coefficient is low, it can dissolve a great number of alloy elements to form a supersaturated solid solution with lattice distortion and lead to the solution strengthening. The WC content of A_1 and A_2 is low and few second phases are formed, so the major strengthening method is solution strengthening. However, the effect of solution strengthening fades away because the α-Co will undergo lattice shear at room temperature, transforming to ε-Co with a hexagonal close-packed structure. In order to enhance the effect of solution strengthening, the scope of the face-centred cubic austenite structure transforming should be enlarged. Meanwhile, the content of alloy elements of the solid solution should be increased to pin dislocations by enhancing the stacking fault energy of the Co-based adhesive phase. As shown in Fig. 2, it can be found from the EDS results of the spray welding layer that the proportion of W in the matrix phase of the solid solution gradually rises with the increasing of the WC content and stabilises in the range of 18.00–19.59%. The Fe_6W_7 phase obtained in spray welding layers A_3, A_4, A_5 demonstrates that the content of Fe_6W_7 also rises with the increasing of W content, which restrains the transformation of α-Co phase to some extent.

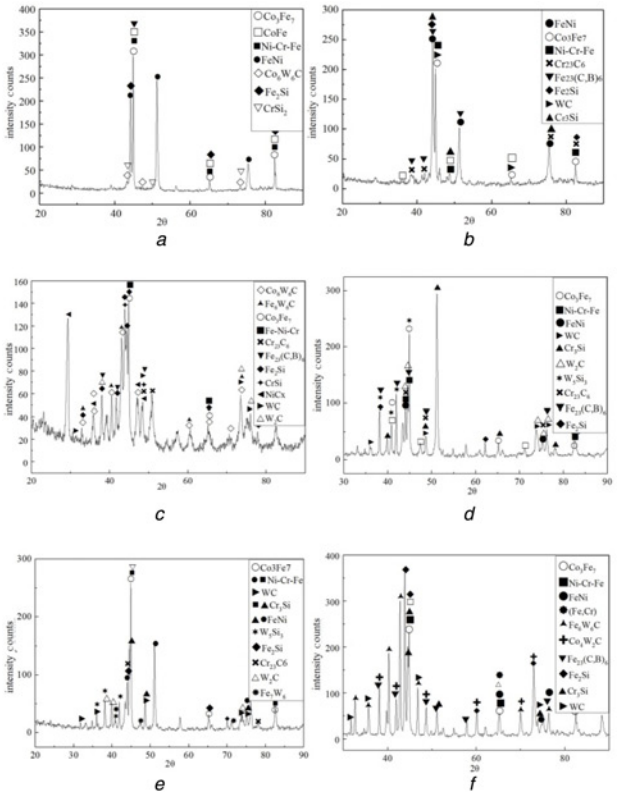

Fig. 1 *X-ray diffraction patterns of Co-based alloys by plasma-transferred arc welding*
a A_1
b A_2
c A_3
d A_4
e A_5
f A_6

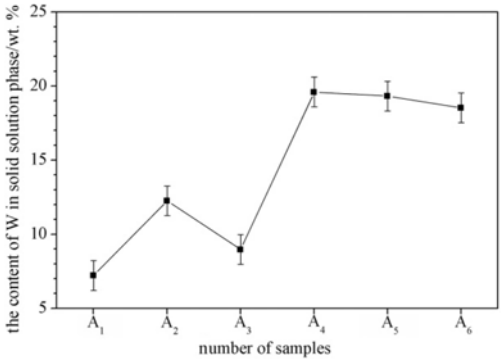

Fig. 2 *Content of W in α-Co solid solution of spray welding layers A_1–A_6 (wt%)*

3.2. Effect of alloy elements: The alloy elements are of crucial importance in the strengthening of the spray welding layer. An effect of second phase strengthening is attained when alloy elements fuse into the spray welding layer and then precipitate. Therefore, melting and precipitating behaviours of alloy elements such as W, C, Si and B influence the strengthening effect of the alloy.

3.2.1. Melting and precipitating behaviour of WC: WC is mainly melted by the way of diffusion. During the process of spray welding, the edges and corners of WC particles are melted preferentially from outside to inside. With the melting process proceeding, WC which has already melted diffuses away from the centre

doi: 10.1049/mnl.2018.5545

of WC particle. Part of the melted WC mix with substrate adequately, the rest which is close to the centre of the particle is diluted by Cr, Ni, Co and F elements.

Based on large numbers of experiments, four types of typical morphologies of the spray welding layer are found, shown as Fig. 3. Fig. 3*a* shows the intergranular eutectic precipitated W-rich phase with an amorphous form. Fig. 3*b* shows a fine W-rich phase, which is radially distributed on the surface of the substrate. Fig. 3*c* shows not only the intergranular precipitated W-rich phase but also the coarse W-rich phase precipitated among the matrix phase. Fig. 3*d* only shows independent and coarse W-rich phase, which exists in the matrix phase.

The EDS results of each marked point in Fig. 3 are shown in Table 4. The variation of W content is greatest in W-rich phase of different morphologies. When little WC melted, like Fig. 3*a*, W-rich phase mainly precipitates along the surface of the intergranular precipitated phase. When WC is melted more and more in the first melting form and diffuses adequately like Fig. 3*c*, the W-rich phase in spray welding layer gradually precipitates in the shape of fine damascene. With the content of melted WC continually rising, the WC is melted in the second melting form. The diluted W-rich phase mainly precipitates on the surface of the matrix phase and has a certain shape like Fig. 3*b*. However, when the content of melted WC exceeds a certain limitation of concentration, the W-rich phase precipitates in the shape of a polygon and grows non-directionally. The concentration of W outside the matrix phase is very high. None or little intergranular precipitation of W-rich phase can be found.

In conclusion, the precipitation morphologies of W-rich phase are relevant to the content of W. With the increasing of W, the morphologies evolve as an amorphous form, damascene shape, star-like shape, and polygon.

3.2.2. Effect of C: The content of WC in the spray welding layer is different because of the powder with different proportion. Thus, the content of C fused into the spray welding layer is different. With the increasing of the C, there are significant changes in two aspects. Firstly, the content and types of eutectic carbide in the spray welding layer increases. Few Co_6W_6C phases, intermediate phase lack carbon, are found in the spray welding layers A_0 and A_1 when the content of WC is low, while no Co_6W_6C phase is found in A_2, A_3, A_4, and A_5. $Cr_{23}C_6$ and $Fe_{23}(C, B)_6$ phases are formed due to the co-ring of Cr, Fe, B and the eutectic of melted carbon. In the spray welding layer A_6, no $Cr_{23}C_6$ phase is found because of the low degree of decomposition of melted WC, which means there is little carbon to utilise, and Fe_6W_6C, Co_4W_2C, and $Fe_{23}(C, B)_6$ phase are mainly formed in the spray welding layer. Secondly, the addition of carbon changes the solidification mode of the spray welding layer. The spray welding layer A_0 with no WC has a simplex crystallisation structure, mainly including α-Co-based solid solution and dendrite-shaped precipitate ($CrSi_2$ + Co solid solution + little tungsten-rich phase), the solution strengthening is the main strengthening method in the spray welding layer. The degree of heterogeneous nucleation of spray welding layer is increased due to the carbon fused into spray welding layer. The heterogeneous nucleation becomes the main way for alloy melt to crystallise. Comparing the binary phase diagram of Co–Cr, Co–Fe, and Cr–C, it can be found that when the content of Fe is 55% the solidus temperature is 985°C. It is shown by the binary phase diagram of Co−Cr that the lowest crystallisation temperature is 1460°C when the content of Cr is 30 wt%. Also, the lowest crystallisation temperature of Cr–C is 1471°C. The forming temperature of Co–Fe solid solution phase is lower than the crystallisation temperature of Co–Cr, the interval of crystallisation temperature increases. With the increasing of the C, the crystallisation of the Cr–C phase gradually plays the dominant role. The strengthening effect of secondary precipitates is more and more obvious.

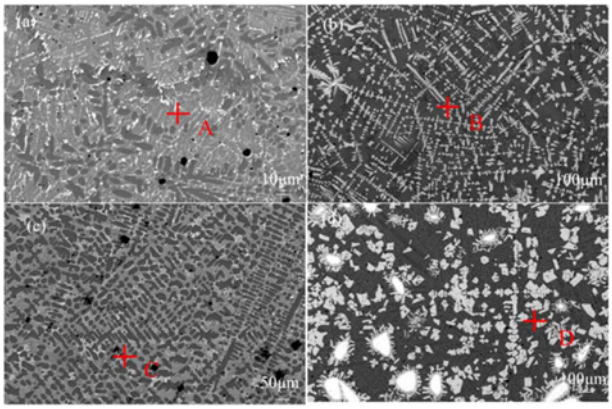

Fig. 3 *Scanning electron microscopy images of four types of typical morphologies of a spray welding layer*
a A_2
b A_3
c A_4
d A_5

Table 4 EDS results of the spray welding layer (wt%)

	Co	Cr	Ni	Fe	W	C
a	24.03	23.23	09.12	17.18	26.20	0.04
b	13.09	13.09	04.94	12.28	53.05	0.03
c	13.56	14.49	03.32	29.22	39.37	0.04
d	07.70	06.58	02.49	16.69	66.51	0.04

3.2.3. Effect of other elements: As the substrate element, Fe influences the spray welding layer in the following two ways. For one thing, the melting of Fe transforms the alloy system from Co–Cr–W–Ni to Co–Cr–Fe–Ni–W. The solid solution phase of the spray welding layer changes from a Co–Cr solid solution to Co–Fe and Fe–Ni solid solutions. An increase of the crystallisation temperature range and a decrease of the crystallisation temperature caused by Co–Fe solid solution is conductive to the forming of the precipitated phase. For another, when the content of Fe reaches a certain concentration, it contributes to the precipitating of Si and formed Fe_2Si phase, which grows directionally in the spray welding layer as the Laves phase. As shown in Fig. 4, solid solutions of Co, Cr, Fe, and Ni exist simultaneously in the Laves phase.

Element Si also plays an important role in the solidification process of the spray welding layer. The intermetallic compounds

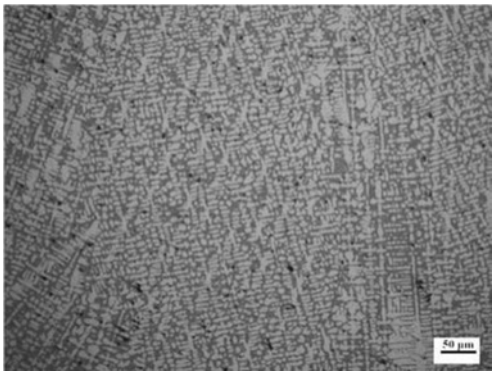

Fig. 4 *Microstructure of the plasma spray welding layer A_3*

such as $CrSi_2$ and Cr_3Si are formed by elements Si and Cr, causing the effect of dispersion strengthening. Meanwhile, the existence of silicon is the main reason why the Laves phase (Fe_2Si) forms. As a kind of intermetallic compound, Laves phase (Fe_2Si) distributed in the spray welding layer leads to a strengthening effect.

4. Conclusions

(i) The main reasons for the strengthening of spray welding layer are the dispersion strengthening caused by eutectic precipitated carbide and silicide and the solution strengthening formed by α-Co with supersaturated W. The proportion of solid solution of W in α-Co steadily ranges from 18 to 19.59%.

(ii) The precipitation morphologies of the W-rich phase are relevant to the content of W, with the increasing of the W, the morphologies evolve as an amorphous form, damascene shape, star-like shape, and the polygon. Amorphous W-rich phase can be obtained when the content of WC ranges from 20 to 30%, evenly distributed W-rich phase in the shape of damascene can be obtained when the WC content ranges from 30 to 40%, and the polygonal W-rich phase can be obtained at the percentage of 40–50%.

5. Acknowledgments: This work was supported by the Natural Science Foundation of Shandong Province (grant no. ZR2016EEQ03) and the Natural Scientific Research Innovation Foundation in HIT (grant no. HIT.NSRIF.201703).

6. References

[1] Lu J.Z., Deng W.W., Luo K.Y., *ET AL.*: 'Surface EBSD analysis and strengthening mechanism of AISI304 stainless steel subjected to massive LSP treatment with different pulse energies', *Mater. Charact.*, 2017, **125**, pp. 99–107

[2] Myalska H., Michalska J.K., Moskal G., *ET AL.*: 'Effect of nano-sized TiC powder on microstructure and the corrosion resistance of WC–Co thermal spray coatings', *Surf. Coat. Technol.*, 2017, **318**, pp. 270–278

[3] Tran A.T.T., Goutier S., Vardelle A., *ET AL.*: ' Microsecond-scale formation of Ni, Ti intermetallics in thermal spray coatings', *Surf. Coat. Technol.*, 2017, **321**, pp. 425–437

[4] Zhang M., Zhou X., Yu X., *ET AL.*: 'Synthesis and characterization of refractory TiZrNbWMo high-entropy alloy coating by laser cladding', *Surf. Coat. Technol.*, 2017, **311**, pp. 321–329

[5] Arias-González F., Val J.D., Comesaña R., *ET AL.*: 'Laser cladding of phosphor bronze', *Surf. Coat. Technol.*, 2017, **313**, pp. 248–254

[6] Yang Z., Wang A., Weng Z., *ET AL.*: 'Porosity elimination and heat treatment of diode laser-clad homogeneous coating on cast aluminum–copper alloy', *Surf. Coat. Technol.*, 2017, **321**, pp. 26–35

[7] Cai C., Chang S., Zhou Y., *ET AL.*: 'Microstructure characteristics of EB-PVD YSZ thermal barrier coatings corroded by molten volcanic ash', *Surf. Coat. Technol.*, 2016, **286**, pp. 49–56

[8] Cao X.Y., Zhu P., Liu T.G., *ET AL.*: 'Thermal aging effects on mechanical and electrochemical properties of stainless steel weld overlay cladding', *Surf. Coat. Technol.*, 2018, **344**, pp. 111–120

[9] Huang S., Sun D., Wang W., *ET AL.*: ' microstructures and properties of in-situ TiC particles reinforced Ni-based composite coatings prepared by plasma spray welding', *Ceram. Int.*, 2017, **41**, (9), pp. 12202–12210

[10] Demian C., Denoirjean A., Pawłowski L., *ET AL.*: 'Microstructural investigations of $NiCrAlY + Y_2O_3$, stabilized ZrO_2, cermet coatings deposited by plasma transferred arc (PTA)', *Surf. Coat. Technol.*, 2016, **300**, pp. 104–109

[11] Acevedo-Dávila J.L., Muñoz-Arroyo R., Hdz-García H.M., *ET AL.*: 'Cobalt-based PTA coatings, effects of addition of tic nanoparticles', *Vacuum*, 2017, **143**, pp. 14–22

doi: 10.1049/mnl.2018.5545